Biomedical Microdevices (2018) 20:45
https://doi.org/10.1007/s10544-018-0290-8

Robust label-free microRNA detection using one million ISFET array

Anurup Ganguli[1,2] · Yoshihiko Watanabe[2] · Michael T. Hwang[2] · Jui-Cheng Huang[3] · Rashid Bashir[1,2,4]

Abstract
Detection of nucleic acid molecules is one of the most pervasive assays in biology, medicine, and agriculture applications. Currently, most comely used DNA/RNA detection platforms use fluorescence labeling and require lab-scale setting for performing the assay. There is a need for developing less expensive, label-free, and rapid detection of biomolecules with minimal utilization of resources. Use of electrical approaches for detection of biomolecules by utilizing their inherent charge is a promising direction for biosensing assays. Here, we report a 1024 × 1024 array of Ion Sensitive Field Effect Transistors (ISFET) as label free sensors for detection of nucleic acid molecules. Using PNA probe functionalized on these ISFET array, we robustly detected miRNA Let-7b by measuring changes in drain current after hybridization of target molecules with concentration as low as 1 nM. We demonstrate that mismatched or non-complementary target molecules resulted in statistically smaller changes. Most importantly, the high-density sensor array shows unprecedented reliability and robustness with P values <0.0001 for all experiments. Practical implementation of this platform could have a wide range of applications in high-throughput nucleic acid genotyping, detection of amplified pathogenic nucleic acid, detection of cell-free DNA, and electrical readouts for current hybridization-based DNA biomolecular assays.

Keywords Electrical DNA sensor · Electrical microarray · Multiplexed biosensing · 1024 × 1024 array · ISFET

1 Introduction

The detection of DNA and RNA molecules is of paramount interest for diagnostics, environmental monitoring, and personalized and precision medicine (Barany 1991; Maehashi et al. 2004; Wang et al. 1997). Microarray revolutionized the nucleic acid detection market using top-down semiconductor fabrication technology allowing thousands of target molecules to be interrogated simultaneously (Wang et al. 2002). However, microarrays require fluorescent labeling and laboratory scale settings such as fluorimeters or laser scanners to read out and transduce optical signals (Batista et al. 2008). Lab-on-chip-based diagnostic and detection of nucleic acids can help achieve miniaturized sensors that can be used at the point of care at doctor's office, hospital bedside, or pharmacies. Electrical detection of biomolecules can be of great interest as it can enable further miniaturization of the instrumentation needed for detection and performing the assays (Hwang et al. 2016; Kaisti 2017; Salm et al. 2014). A field effect transistor (FET) is a strong candidate as a miniaturized biomolecular sensor that can provide highly sensitive and specific detection of nucleic acids. Also, FET based biosensor technology does not need fluorescence labeling and optical components as it directly reads and transfers electrical signals to computer and personal electronics. Compatibility with CMOS fabrication process allows easy miniaturization and integration of a high-density array on a single chip.

Electronic supplementary material The online version of this article (https://doi.org/10.1007/s10544-018-0290-8) contains supplementary material, which is available to authorized users.

✉ Rashid Bashir
rbashir@illinois.edu

[1] Department of Bioengineering, University of Illinois at Urbana-Champaign, 1304 W Springfield Ave, Urbana, IL 61801, USA

[2] Micro and Nanotechnology Laboratory, University of Illinois at Urbana-Champaign, 208 N. Wright St, Urbana, IL 61801, USA

[3] Taiwan Semiconductor Manufacturing Company, 9 Creation Rd, Hsinchu Science Park, Hsinchu, Taiwan, 300-77, Republic of China

[4] Carle Illinois College of Medicine, 807 South Wright Street, Champaign, IL 61801, USA

Published online: 02 June 2018

Therefore, FET based biosensor can eliminate many limitations of current technologies. Many examples of arrayed electrical biosensors have been reported using planar silicon FETs, silicon nanowire, carbon nanotube and 2 dimensional materials such as graphene and MoS_2 (Batista et al. 2008; El-Grour et al. 2018; Gao et al. 2016; Hwang et al. 2016; Souteyrand et al. 1997; Star et al. 2006). However, none of these approaches has yet shown a very large number of devices in an array to allow for statistically robust detection. Moreover, reproducibility and reliability have been major issues for the abovementioned arrays, as 1-D and 2-D materials suffer from heterogeneity over the sensing area and poor reproducibility between batches. This makes planar Si-based FET an attractive platform for practical development and commercialization of an electrical biosensing technology. We have recently reported pH detection using a massively parallel ion-sensitive field-effect transistor (ISFET) array (Abdolkader and Alahdal 2018; Duarte-Guevara et al. 2017). Our chips are fabricated in a commercially available foundry and thus offer consistent manufacturing and reliability (Duarte-Guevara et al. 2014). Using this array, we have already shown pH sensing and pH based detection of nucleic acid amplification from foodborne bacterial pathogens (Duarte-Guevara et al. 2017; Duarte-Guevara et al. 2016). We now present an array of over million ISFETs as an electrical DNA chip array on a 7×7 mm^2 area with unprecedented reliability and robustness. Since a large number of transistors can be assigned to, or example, a single reaction and detection allowing for uncertainty in measurements to be reduced significantly and achieve statistical robustness (P values << 0.0001). Moreover, the large sensing array can also allow for forming a large array of spotted probes to form an electrical analogue of a microarray.

The optical image and the schematic of the measurement system is shown in Fig. 1. The structure and fabrication process of the array chip were reported earlier (Duarte-Guevara et al. 2017). The sensing element is a double gated SOI (Silicon on Insulator) transistor with a Hafnium Oxide (HfO_2) dielectric exposed to the fluid for molecular functionalization [13]. To investigate the electrical properties of our FET devices, the output and transfer characteristics were measured prior to the functionalization of the PNA probe. As shown in Fig. 1c, typical I_{ds} versus V_{gs} curves were obtained and showed only a small variation over the million sensing array. The standard deviation of I_{ds} across all 1024×1024 pixels at $V_{fg} = 1.7$ was as low as 1.463 μA which is less than 13% of the mean. The various RNA detection experiments in this work were performed at a similar biasing voltage. The HfO_2 gate dielectric sensing area was functionalized with PNA probe using (3-Aminopropyl)triethoxysilane (ATPES) and glutaraldehyde (Fig. 2). For PNA-RNA hybridization detection experiments, microRNA (miRNA) Let-7b was used as a target molecule, which is a biomarker associated with human breast, lung, prostate, and other cancers (Thammaiah and Jayaram 2016). The basic approach for the nucleic acid molecule detection on a sensing pixel is demonstrated in Fig. 1d. The source-drain current was measured before and after the hybridization, and ΔI_{ds} was calculated. For the specificity and negative control tests, miRNA-21 was used as the non-complementary RNA (Boele et al. 2014; Kalofonou and Toumazou 2014). To take advantage of the large sensing area of the array, different test conditions such as different concentration and other nucleic acids were measured on the same chip. Sequences of nucleic acids used in the experiments are presented in Table 1.

2 Methods

2.1 Chip fabrication

The FET array was fabricated at Taiwan Semiconductor Manufacturing Company (TSMC) with a process that was reported earlier (Duarte-Guevara et al. 2017) In short, standard metal-oxide-semiconductor (MOS) devices was fabricated in a silicon-on-insulator (SOI) wafer followed by bonding with carrier wafer. The sensing area was opened by lithography and dry-etch step and a hafnium oxide HfO_2 layer was deposited to create sensing membrane of FET sensor. The high-K material, HfO_2 acted as a top-gate dielectric with the buffer solution. A cross-sectional schematic of one pixel is presented in Fig. 1d. The decoder is integrated in the devices, which enables the read-out the current of 1024 X 1024 of pixels in series. The integrated chip then connected to the PCB with wire-bonds.

2.2 Testing setup

The integrated chip with PCB was connected with a PXI logic IC tester (OpenATE, Hsinchu, Taiwan). The IC tester controlled the decoder to select pixels and set bias conditions. The drain current of each pixel was then amplified and recorded. The measurement process is coordinated with custom-built software and recorded in CSV format in a personal computer.

2.3 Probe functionalization

The chip was cleaned with O_2 plasma for 3 min. Then the chip was reacted with 2% APTES in a beaker for 2 h. After rinsing with ethanol and DI water, the chip was soaked into 2.5% glutaraldehyde for 1 h. A square PDMS well was placed on the chip to localize the probe. 10 μM of the PNA probe was added into the PDMS well and kept for overnight at room temperature.

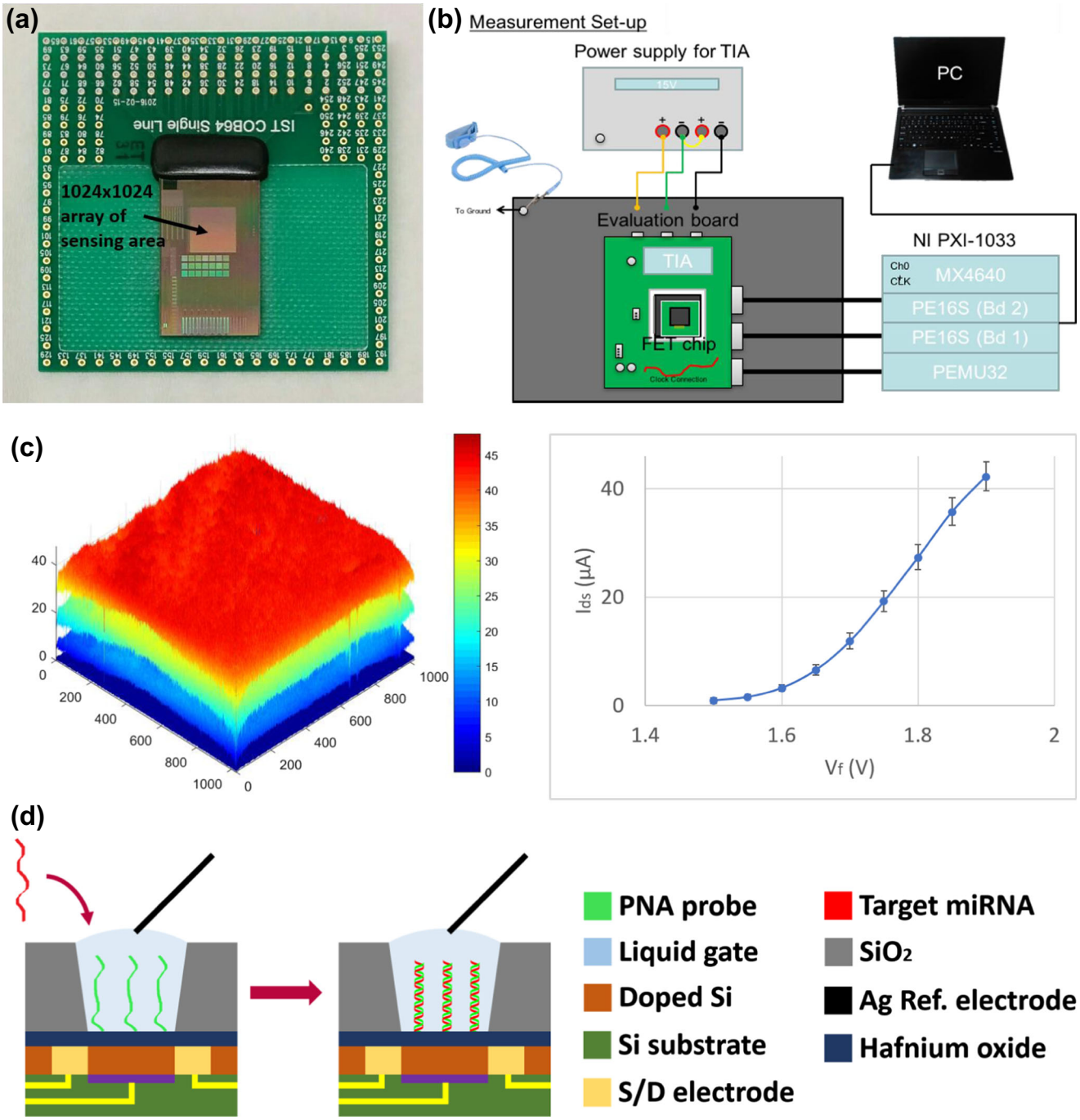

Fig. 1 A million FET sensor array chip image and the measurement set up. **a** Top-view of the sensor array. The black arrow indicates the 1024 × 1024 array in 7 × 7 mm^2 sensing area. **b** The testing setup describing the PCB, TIA (transimpedance amplifier) and wire-bonds to PCB. **c** 3D map (left) and overall population (right) of whole array of drain-source current as a function of V_{fg}. The error bars are one standard deviation. **d** Schematic cross-section of one sensor pixel. The relevant structures and components are color-coded on the right

2.4 Electrical measurement of hybridization events on a chip

The chip was rinsed with SSC buffer solution to remove non-specifically absorbed probes. Then the chip was measured with DI-water at $V_{fg} = 1.7\sim2.0$ V. The hybridization was conducted by adding complementary or mismatched RNA with concentrations from 1 nM to 1 μM and incubated for 30–60 min in the PDMS reservoir on the FET chip. Then, the chip was rinsed gently with DI water. I-V curves and resistance were measured by the experimental settings mentioned above in DI

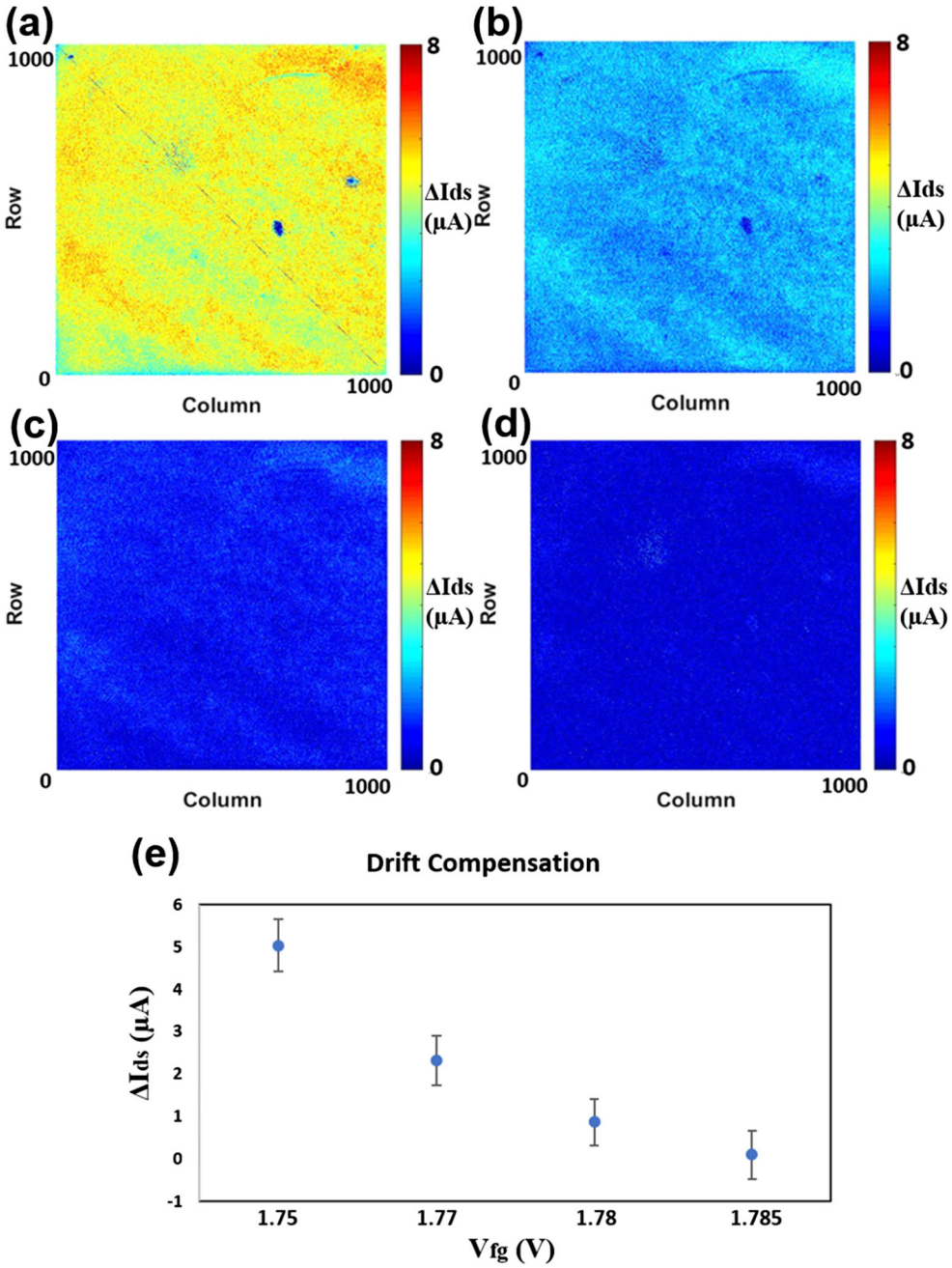

Fig. 2 Real-time drift compensation of the 1024 × 1024 biosensor array. **a** After adding DI water as a liquid gate on the sensing area ΔI_{ds} was measured at $V_{fg} = 1.75$ V before and after 1 h The array showed non zero ΔI_{ds} with a spatial variation owing to the drift effect. **b** ΔI_{ds} was measured again with a new biasing voltage of $V_{fg} = 1.77$ V for the 1 h measurement. The spatial map shows reduced ΔI_{ds} values. **c** At $V_{fg} = 1.78$ V, the map showed a a very small variation and drift was almost compensated. **d** Drift was completely compensated with very little spatial variation at $V_{fg} = 1.785$ V. The scale represents ΔI_{ds} in μA. **e** Graph shows the real-time drift compensation as reducing ΔI_{ds} values with different biasing voltages. Mean of $\Delta I_{ds} \sim 0$ for $V_{fg} = 1.785$ marks the completion of real-time drift compensation process. The error bars are standard deviation

water. Ag/AgCl electrode was used as a gate electrode, which swept fluid voltage (V_{fg}) to the buffer solution directly.

Table 1 Sequences used in the experiments

Name	Sequences (5′ to 3′)
PNA probe	N-AACCACACAACCTACTACCTCA-C
Let-7b	UGAGGUAGUAGGUUGUGUGGUU
miRNA-21	UAGCUUAUCAGACUGAUGUUGA

3 Results and discussion

The array of silicon FETs was fabricated at Taiwan Semiconductor Manufacturing Company (TSMC) foundries following the previously reported methods (Duarte-Guevara et al. 2017). Briefly, SOI (Silicon on Insulator) was used as an active channel and each of the FET was isolated by SiO_2. Top gate voltage was applied from the fluid above the sensor using a Ag/AgCl electrode (fluid gate). Back-gate to the channel was also available and biased at a fixed voltage. Notably, in our FET arrays, a high-k dielectric material, hafnium oxide, was deposited by ALD over the entire chip area, creating the

FET sensing membrane. This high-k dielectric reduces ion transport across the dielectric as compared to the traditional top gate dielectrics such as silicon dioxide (Dorvel et al. 2012). Dimension of each of the pixel was 7×7 μm^2 and the whole sensing area was 7×7 mm^2, which is comparable in size with a conventional high-density microarray chips. The schematic of the sensor structure is presented in Fig. 1a. The top-view of the architecture is shown in Fig. 1 and includes sensing area, row/column decoders, and wire-bonds to PCB. Further details on the specific dimensions and electrical characterization of the ISFET was reported in our prior publication (Duarte-Guevara et al. 2017).

The FET chip was connected to a PXI logic IC tester. The tester established communication with a Spectrum transient recorder (Spectrum, Grosshansdorf, DE). The decoding circuits selected each FET and controlled the biasing voltage. The measurement of the entire 1024×1024 array of FETs was performed in approximately 90 s. The measurement data was transferred via a customized MTS3 software in a comma separated values (csv) file format for later analyses. The scheme of the setup is in Fig. 1b.

To create a solution reservoir of the buffer solution as a liquid gate, a 400 μL PDMS well was bonded on the chip leaving the sensing area open. The basic characterization of the BioFETs was performed before the nucleic acid detection tests. Figure 1 shows the transfer characteristics of FET array as a function of the drain current (I_{ds}) vs. fluid-gate voltage (V_{fg}). V_{fg} was swept from 1.5 to 1.9 V with a constant drain voltage of 2 V to obtain transfer curves. Figure 1c is an overlaid 3D graph of the multiple drain currents of each sensor with different V_{fg} biasing values. There is a 'dummy diagonal' sensors reference line that is used for validation of the chip fabrication and performance. Figure 1 presents the transfer curve of standard transistor characteristics for the entire array (excluding dummy pixels) and shows very low standard deviation across all the sensors in the array.

FET based biosensors can be vulnerable to effect of temperature changes, hysteresis, and drift (Kalofonou and Toumazou 2014). When using DI water as a fluid gate, a drift, can be observed versus time without applying any voltage or adding charged biomolecules. In this work, the drift effect and its compensation have been carefully studied and used to optimize our measurement/sensing protocol. Even though some spatial variations were observed across the chips, the performance of these foundry-fabricated sensors is highly robust.

To study the drift in sensors over time, we simulated a negative control (no nucleic acid) reaction by adding only DI water on the sensor array. Then, I_{ds} was measured at a fluid

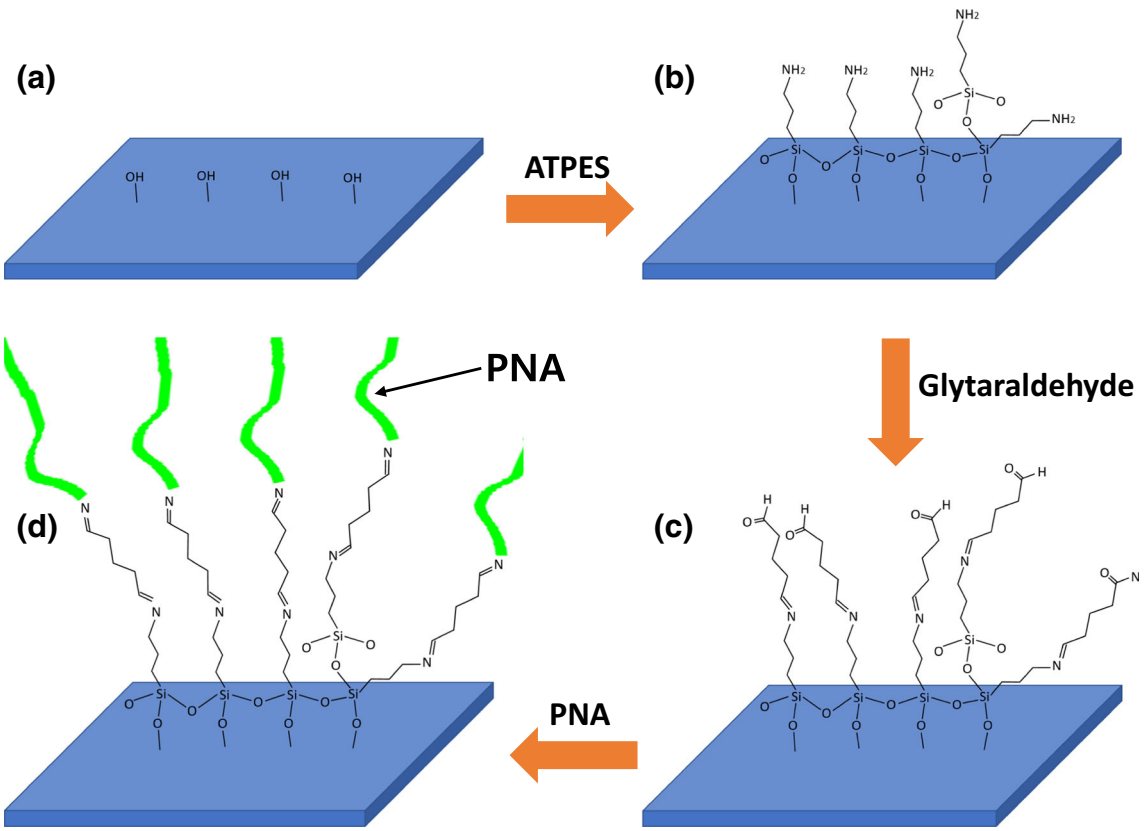

Fig. 3 Schematic of the surface functionalization of the HfO_2 for miRNA sensing (**a**) The hafnium oxide surface was hydroxylated by O_2 plasma. **b** The surface was then silanization by APTES. **c** Covalent bonding between the Amide group and glutaraldehyde. **d** PNA functionalization with the amide group in glutaraldehyde

gate voltage V_{fg} of 1.75 V at time 0 and after 1 h of exposure of the sensors to the DI water. Changes in this drain current (t_{1hour} -t_0) is shown as a color map in Fig. 2a and shows the spatial variation over time in the transistor current due to drift. To compensate or correct for this drift, we varied the biasing voltage at the 1 h measurement until the change in drain current became 0 for all the transistors in the array. The results of drift compensation at different biasing voltages is shown in Fig. 2b–d. At 1.785 V (Fig. 2d), the spatial variation and pseudo-field effect was clearly compensated. The summary of the drift compensation is shown in Fig. 2e with mean and standard deviation graph of ΔI_{ds}. This drift compensation was possible for our array since the drifts of the individual FETs in the array was tied together. This also implies that one region of the array can be kept as a negative control (no nucleic acid) and real-time drift correction for this region would compensate the drift effects for the entire array. After the compensation, measurement conditions were very stable and conducive for detection of biomolecular binding events over the entire array. If uncorrected, the drift can result in false-positive signals affecting the sensitivity of the assay (Bergveld 1986). Thus, it is important to utilize the reference sensing area to compensate for the drift values, and this compensation is easily possible with our large sensor array. This unique real-time drift correction feature of our platform allows drift compensation at any data collection time point making our assay immune to drift effects.

After the basic characterization of the chips, the actual nucleic acid detection experiments were performed. In order to take advantage of the sensor array, different concentrations of target molecules were tested on the same chip at the same time. This was possible not only because the chip has a large sensor array but also because the variation in characteristics of each FET was very small. To conduct multiple experiments on one chip, a PDMS well with 9 holes which served as separate reaction chambers, was used for the nucleic acids detection experiments. A picture of the experimental setting including the PDMS well is shown in Fig. S1. PNA was chosen as the

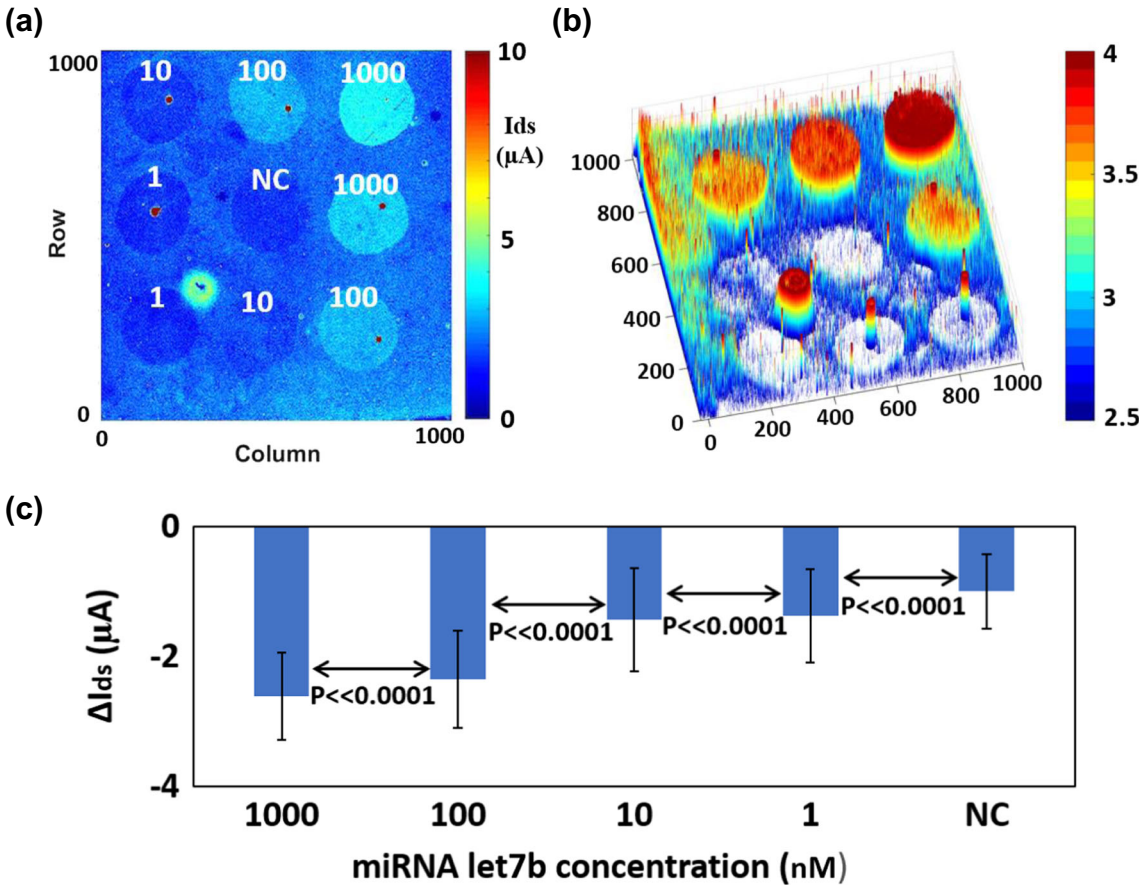

Fig. 4 miRNA-let7 detection on the FET array. **a** Heat map of drain current with different concentrations of target RNA in the array. The numbers in white represent concentrations of the target in nM. NC is negative control where no nucleic acid target was present. **b** 3D plot of (**a**). The scale of the color code in (**a**) and (**b**) represents I_{ds} in μA. There are some spots resulting in noise but given the large number of pixels, the noise can easily be removed and eliminated. **c** Change of I_{ds} curve as a function of the target Let7b concentration. The NC shifts the I_{ds} significantly less. Statistical values (means ± standard deviation) were based on each circled area indicated in (**a**). The range of *p*-values are indicated with arrows

probe molecule since PNA does not contain a charged phosphate backbone, making the binding between PNA and other nucleic acids stronger than that between DNA/DNA or DNA/RNA strands even in low salt conditions (Batista et al. 2008; Maehashi et al. 2004). Moreover, uncharged PNA molecules do not result in electrical modulation of the semiconductor channel unless the target hybridization occurs, thus eliminating any background electrical noise issues from the probe molecule itself (Kim et al. 2016; Maehashi et al. 2004; Zhang et al. 2008). To functionalize the surface of the chip with PNA probes, the hafnium oxide surface was hydroxylated by O_2 plasma. The surface was then treated with (3-Aminopropyl)triethoxysilane solution (APTES – 2% ethanol) for silanization and then reacted with glutaraldehyde (2.5%) to generate a self-assembled monolayer with terminal aldehyde group. This terminal aldehyde group is then covalently bonded with amine group at the 5′ side of PNA probe (Fig. 3) (Gaylord et al. 2002; Kalofonou and Toumazou 2014). The sensor array at this stage is ready for target hybridization.

The sensitivity of the FET array biosensor was investigated by conducting hybridization of various concentrations of complementary RNA strands on the PNA-functionalized FET devices, are shown in Fig. 4a. DI water was used as the reference negative control. Figure 4b shows a 3D electrical plot of the drain current matrix presenting the multiple drain currents versus different concentrations of target strands, along with the negative control. As the chip has large number of sensors in the array, variance between each was also assessed. Figure 4c shows the summary of shifts of I_{ds} at the corresponding concentrations, which shows that ΔI_{ds} is dependent on the concentration of the complementary RNA. The number of molecules attached on the 2D surface is a function of the concentration of the molecules in the solution above the FET and has been modelled in the past using a diffusion-reaction model (Dak et al. 2016; Nair and Alam 2010; Salm et al. 2013; Squires et al. 2008). We found a detection limit of 1 nM based on the signal that exceeds the background level by 37.5% difference (p value<<0.0001). This detection limit is comparable to what is used in the current microarray

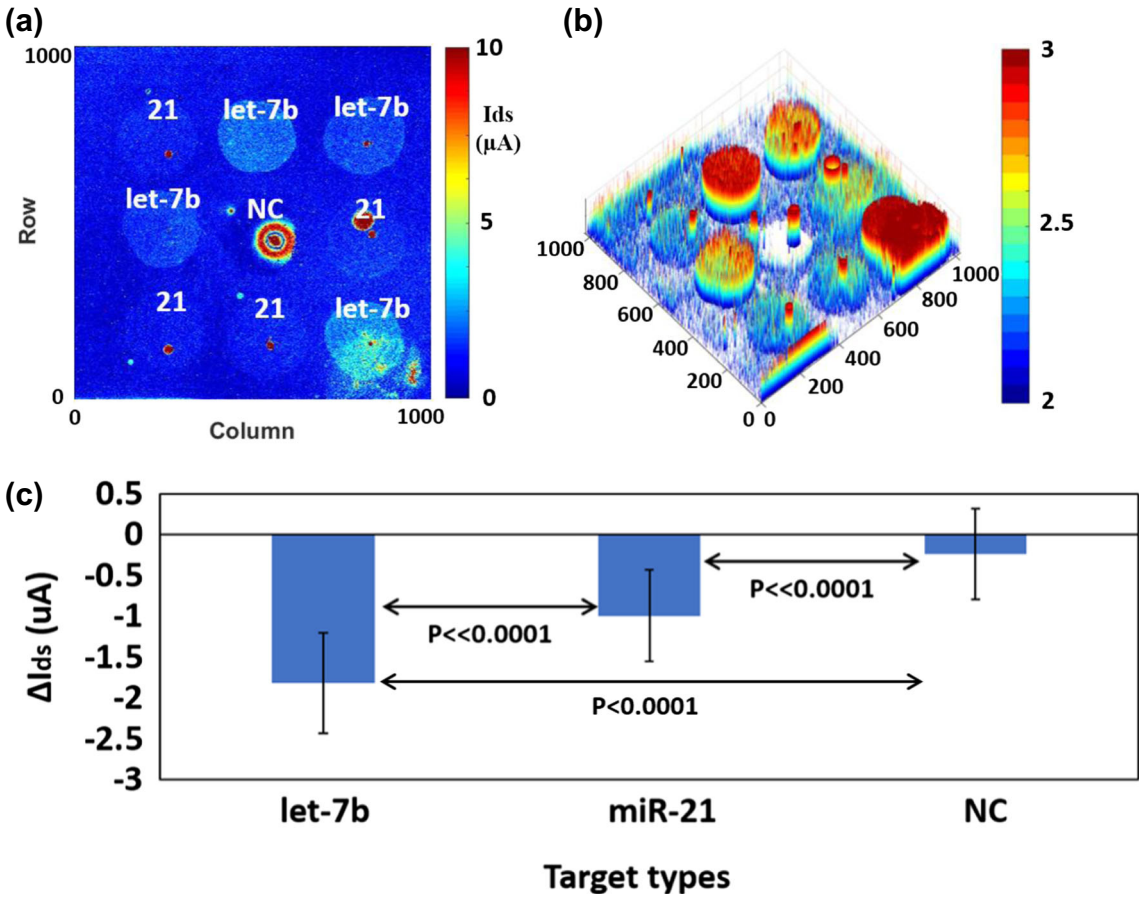

Fig. 5 Specificity test with perfect matched (Let-7b) and non-complementary miRNA (miR-21). **a** Heat map of drain current of the array with different target and non-complementary RNA. The white numbers represent types of the target, 21 is miR-21. NC is negative control; no target was treated. **b** 3D plot of (**a**) The scale of the color code in (**a**) and (**b**) represents I_{ds} in μA. Summary of shift of I_{ds} curves. The miR-21 shifts the I_{ds} significantly less. Statistical values (means ± standard deviation) were based on each circled area indicated in (**a**). The range of p-values are indicated with arrows

technology with fluorescent detection (Hong et al. 2005). However, as shown in the Fig. 4c, the *P* values of results are less than 0.0001 indicating that this array sensor is extremely reliable and is robust against noise artifacts even with this method of electrical detection.

The Debye length should be considered when detecting electrical charge in ionic solution. The Debye length represents the distance over which the charge is shielded in an ionic solution – the counter-ions in the solution can shield the original charge (Maehashi et al. 2004). In the 1X SSC solution, which is generally used as a buffer solution, the Debye length is <1 nm. To maximize sensitivity, we used DI water in our experiments for electrical detection after the hybridization process. The use of PNA as the probe allows the PNA-RNA complex to stay intact even at the very low or no salt conditions. To verify the specificity of our biosensor assay, complementary Let7b miRNA and non-complementary miRNA-21 were introduced for hybridization on the PNA-functionalized FET array. Fig. 5 shows transfer characteristics of the PNA-immobilized FET biosensors incubated with 1 μM of Let-7b and miRNA-21. The results show that the shifts of I_{ds} of the FETs for complementary miRNA was much larger and distinguishable ($p << 0.0001$) than that for both the non-complementary RNA and the no target control. The ΔI_{ds} of non-complementary RNA might be caused by a small amount of non-specific adsorption but since our platform has a large number of FETs per reaction even while testing multiple conditions on the same chip (~15,000), the *p*-value for different conditions is very low and highly significant. The data confirms that the biosensors can distinguish the complementary DNA from mismatched RNAs and can be used for miRNA detection.

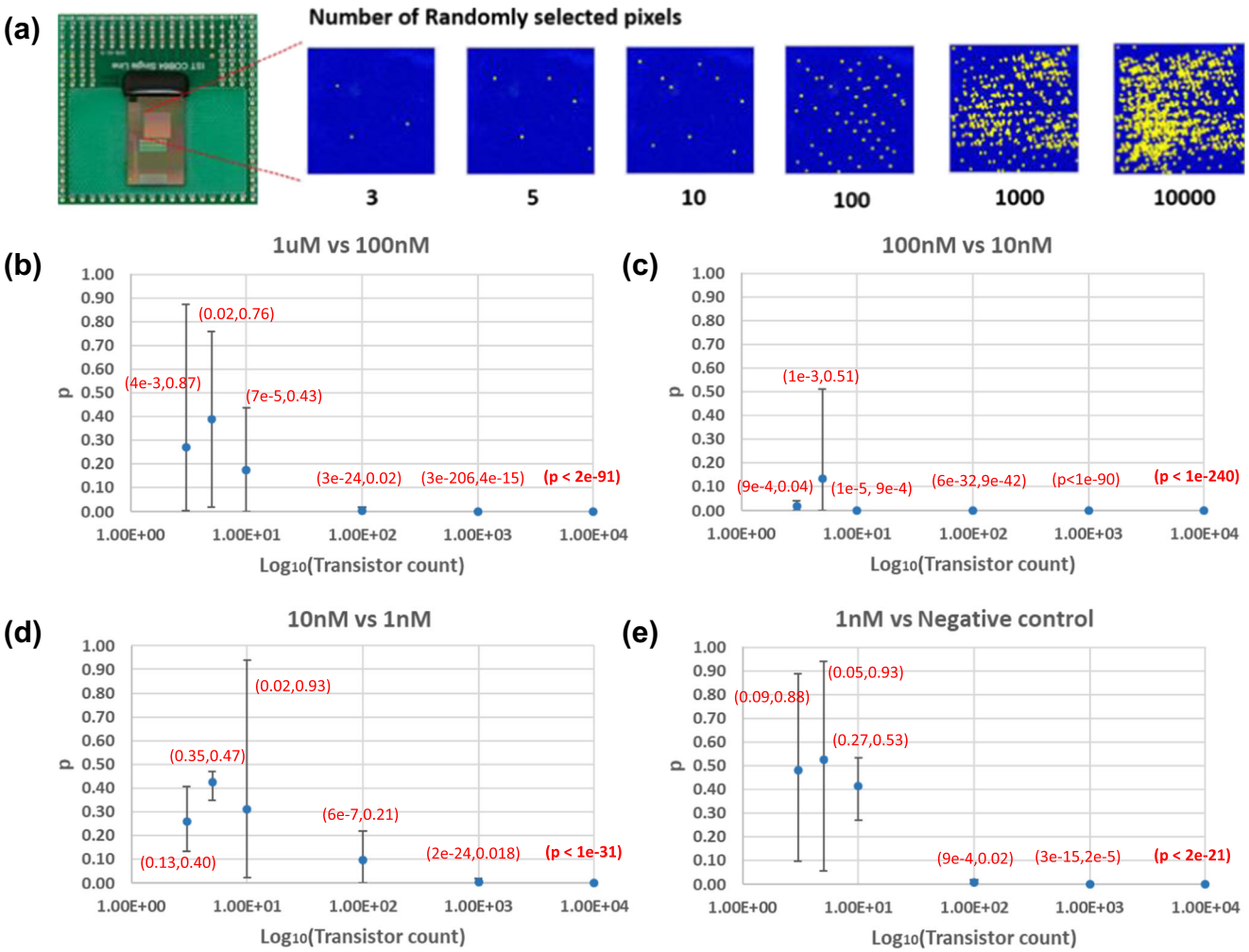

Fig. 6 The effect of large number of transistors on the p-value. The p-values between different test conditions (concentrations) were calculated using student's t-test as a function of number of transistors used in the reaction. **a** The schematic shows the increasing number of the pixels randomly selected for the p-value calculation. **b**–**e** *P*-value graphs comparing two different concentrations as indicated in the top of graphs. For experiments with low number of transistors (3 to 10), the p-value is higher and very variable. As the transistor count per reaction increases, the p-value becomes very low for all test conditions suggesting that the system becomes very reliable and robust against noise artifacts. The error bars are maximum and minimum. The exact range of p-values is mentioned in brackets in red

Finally, to further assess the statistical robustness of our assay, we evaluated the effect of large number of transistors on the p-value in our experiments. Using the limit of detection experiments from Fig. 4, we calculated the p-value between different test conditions (concentrations) as a function of number of transistors used in the reaction. As can be seen from Fig. 6, in our assay the difference between different concentrations and the negative control is highly significant. The plots in Fig. 6b–e show that for experiments with low number of transistors, the p-value is higher and very variable. However, as the transistor count per reaction increases, especially above a few hundred transistors, the p-value becomes very low for all test conditions suggesting that the system becomes very reliable and robust against noise artifacts. The large number of sensors pixels within one fluid well is important as this truly takes advantage of the VLSI silicon fabrication to reduce the p values and increases the reliability and robustness of the sensing. If a small number of devices is used then large p value, reflecting the variability in the molecular binding events, can result in the lack of discrimination across the concentrations of the target molecule.

The original optical microarrays were inspired by VLSI lithography process used in the semiconductor industry to fabricate massive number of micro-sized spots on a chip. Our work here finally demonstrates a prototype of an electrical microarray with more than 1 million FET sensors in a single chip. These sensors would not need fluorescence labeling or optical component, while reducing false-positive signals due to the unprecedented large number of sensors in 1 a chip and within one fluid reaction well. The chip is commercialization-ready since it is foundry based, and shows high reliability, robustness and reproducibility. Further development and implementation of this technology would allow more affordable and accurate diagnosis of myriad of diseases such as cancer, neurodegenerative diseases, cardiovascular disease, and immune dysfunction.

4 Conclusion

Label-free detection of miRNA with high resolution was achieved by using a massively parallel FET array. The PNA modified FET biosensor exhibits limit of detection of 1 nM and can also discriminate between complementary miRNA from mismatched RNAs with high specificity. The work provides a significantly improved platform for biomolecular detection by using foundry based Silicon on Insulator FET technology. It provides high fidelity and reproducibility which has been achieved yet with 1- or 2-D materials such as nanowire, carbon nanotube and graphene because of the inherent heterogeneity of these materials. Our results open the opportunities for the development of more reliable and efficient diagnostic tools such as miniaturized point-of-care biosensors for high-throughput screening to detect potentially life-threatening human diseases, drug discovery, and many other applications.

Acknowledgements We thank the staff at the Micro and Nanotechnology Laboratory at UIUC for facilitating the chip fabrication. The work was funded by NSF grant 1534126 and the University of Illinois at Urbana-Champaign.

Author contributions A.G., Y.W. and R.B conceived the idea and designed the study. A.G. and Y.W., designed and performed the experiments. J.H. assisted with the experiments and provided intellectual inputs. M.H., A.G., Y.W. and R.B wrote and edited the manuscript.

Compliance with ethical standards

Competing interest The authors declare no competing financial interests.

References

T.M. Abdolkader, A.G. Alahdal, Sensors Actuators B Chem. **259**, 36 (2018)
F. Barany, Proc. Natl. Acad. Sci. **88**, 189 (1991)
R. Batista, N. Saibo, T. Lourenço, M.M. Oliveira, Proc. Natl. Acad. Sci. **105**, 3640 (2008)
P. Bergveld, Biosensors **2**, 15 (1986)
J. Boele, H. Persson, J.W. Shin, Y. Ishizu, I.S. Newie, R. Søkilde, S.M. Hawkins, C. Coarfa, K. Ikeda, K. Takayama, K. Horie-Inoue, Y. Ando, A.M. Burroughs, C. Sasaki, C. Suzuki, M. Sakai, S. Aoki, A. Ogawa, A. Hasegawa, M. Lizio, K. Kaida, B. Teusink, P. Carninci, H. Suzuki, S. Inoue, P.H. Gunaratne, C. Rovira, Y. Hayashizaki, M.J.L. de Hoon, Proc. Natl. Acad. Sci. **111**, 11467 (2014)
P. Dak, A. Ebrahimi, V. Swaminathan, C. Duarte-Guevara, R. Bashir, M.A. Alam, Biosensors **6** (2016)
B.R. Dorvel, B. Reddy, J. Go, C. Duarte Guevara, E. Salm, M.A. Alam, R. Bashir, ACS Nano **6**, 6150 (2012)
C. Duarte-Guevara, F.-L. Lai, C.-W. Cheng, B. Reddy, E. Salm, V. Swaminathan, Y.-K. Tsui, H.C. Tuan, A. Kalnitsky, Y.-S. Liu, R. Bashir, Anal. Chem. **86**, 8359 (2014)
C. Duarte-Guevara, V. Swaminathan, B. Reddy, J.-C. Huang, Y.-S. Liu, R. Bashir, RSC Adv. **6**, 103872 (2016)
C. Duarte-Guevara, V. Swaminathan, B. Reddy Jr, C.-H. Wen, Y.-J. Huang, J.-C. Huang, Y.-S. Liu, R. Bashir, Sensors Actuators B Chem. **250**, 100 (2017)
T. El-Grour, M. Najari, L. El-Mir, J. Comput. Electron. **17**, 297 (2018)
Z. Gao, H. Kang, C.H. Naylor, F. Streller, P. Ducos, M.D. Serrano, J. Ping, J. Zauberman, R.W. Rajesh, Y.-J. Carpick, Y.W. Wang, Z. Park, L.R. Luo, A.T.C. Johnson, ACS Appl. Mater. Interfaces **8**, 27546 (2016)
B.S. Gaylord, A.J. Heeger, G.C. Bazan, Proc. Natl. Acad. Sci. **99**, 10954 (2002)
B.J. Hong, V. Sunkara, J.W. Park, Nucleic Acids Res. **33**, e106 (2005)
M.T. Hwang, P.B. Landon, J. Lee, D. Choi, A.H. Mo, G. Glinsky, R. Lal, Proc. Natl. Acad. Sci. **113**, 7088 (2016)
K. Maehashi, K. Matsumoto, K. Kerman, Y. Takamura, E. Tamiya, Jpn. J. Appl. Phys. **43**, L1558 (2004)
M. Kaisti, Biosens. Bioelectron. **98**, 437 (2017)
M. Kalofonou, C. Toumazou, IEEE Trans. Biomed. Circuits Syst. **8**, 565 (2014)
J. Kim, S.-Y. Park, S. Kim, D.H. Lee, J.H. Kim, J.M. Kim, H. Kang, J.-S. Han, J.W. Park, H. Lee, S.-H. Choi, Sci. Rep. **6**, 31984 (2016)

P.R. Nair, M.A. Alam, J. Appl. Phys. **107**, 64701 (2010)
E. Salm, C.D. Guevara, P. Dak, B.R. Dorvel, B. Reddy, M.A. Alam, R. Bashir, Proc. Natl. Acad. Sci. **110**, 3310 (2013)
E. Salm, Y. Zhong, B. Reddy, C. Duarte-Guevara, V. Swaminathan, Y.-S. Liu, R. Bashir, Anal. Chem. **86**, 6968 (2014)
E. Souteyrand, J.P. Cloarec, J.R. Martin, C. Wilson, I. Lawrence, S. Mikkelsen, M.F. Lawrence, J. Phys. Chem. B **101**, 2980 (1997)
T.M. Squires, R.J. Messinger, S.R. Manalis, Nat. Biotechnol. **26**, 417 (2008)
A. Star, E. Tu, J. Niemann, J.-C.P. Gabriel, C.S. Joiner, C. Valcke, Proc. Natl. Acad. Sci. U. S. A. **103**, 921 (2006)
C.K. Thammaiah, S. Jayaram, Non-coding RNA Research. **1**, 77 (2016)
J. Wang, G. Rivas, X. Cai, E. Palecek, P. Nielsen, H. Shiraishi, N. Dontha, D. Luo, C. Parrado, M. Chicharro, P.A.M. Farias, F.S. Valera, D.H. Grant, M. Ozsoz, M.N. Flair, Anal. Chim. Acta **347**, 1 (1997)
D. Wang, L. Coscoy, M. Zylberberg, P.C. Avila, H.A. Boushey, D. Ganem, J.L. DeRisi, Proc. Natl. Acad. Sci. **99**, 15687 LP (2002)
G.-J. Zhang, J.H. Chua, R.-E. Chee, A. Agarwal, S.M. Wong, K.D. Buddharaju, N. Balasubramanian, Biosens. Bioelectron. **23**, 1701 (2008)